Kelvin probe force microscopy of metallic surfaces used in Casimir force measurements

R. O. Behunin,[1] D. A. R. Dalvit,[2] R. S. Decca,[3] C. Genet,[4] I. W. Jung,[5] A. Lambrecht,[6] A. Liscio,[7] D. López,[5]
S. Reynaud,[6] G. Schnoering,[4] G. Voisin,[3,8] and Y. Zeng[2,*]

[1]*Department of Applied Physics, Yale University, New Haven, Connecticut 06511, USA*
[2]*Theoretical Division, MS B213, Los Alamos National Laboratory, Los Alamos, New Mexico 87545, USA*
[3]*Department of Physics, Indiana University–Purdue University Indianapolis, Indianapolis, Indiana 46202, USA*
[4]*ISIS & icFRC, Université de Strasbourg and CNRS, 8 allée Monge, 67000 Strasbourg, France*
[5]*Center for Nanoscale Materials, Argonne National Laboratory, Argonne, Illinois 60439, USA*
[6]*Laboratoire Kastler Brossel, UPMC-Sorbonne Universités, CNRS, ENS-PSL Research University, Collège de France, Campus Jussieu, F-75252 Paris, France*
[7]*ISOF-CNR, via Gobetti 101, 40129 Bologna, Italy*
[8]*Laboratoire Univers et Théories (LUTH), Observatoire de Paris, CNRS UMR8102, Université Paris Diderot, 5 Place Jules Janssen, 92190 Meudon, France*

(Received 14 July 2014; published 11 December 2014)

Kelvin probe force microscopy at normal pressure was performed by two different groups on the same Au-coated planar sample used to measure the Casimir interaction in a sphere-plane geometry. The obtained voltage distribution was used to calculate the separation dependence of the electrostatic pressure $P_{\rm res}(D)$ in the configuration of the Casimir experiments. In the calculation it was assumed that the potential distribution in the sphere has the same statistical properties as the measured one, and that there are no correlation effects on the potential distributions due to the presence of the other surface. The result of this calculation, using the currently available knowledge, is that $P_{\rm res}(D)$ does not explain the magnitude or the separation dependence of the difference $\Delta P(D)$ between the measured Casimir pressure and the one calculated using a Drude model for the electromagnetic response of Au. We discuss in the conclusions the points which have to be checked out by future work, including the influence of pressure and a more accurate determination of the patch distribution, in order to confirm these results.

DOI: 10.1103/PhysRevA.90.062115 PACS number(s): 31.30.jh, 12.20.−m, 42.50.Ct, 78.20.Ci

I. INTRODUCTION

Measurements of the Casimir interaction between gold-covered mirrors now reach a good precision, which opens the way to detailed comparisons with theoretical predictions. Some measurements, performed at distances smaller than 1 μm, lead to unexpected conclusions [1–4]. These results agree with a description of conduction electrons in metals by the lossless plasma model, and deviate significantly from that based on the Drude model which accounts for dissipation [5–8]. Different conclusions are reached in another experiment performed at distances of the order or larger than 1 μm [9]. The results of this experiment agree with predictions drawn from the dissipative Drude model, after the contribution of the electrostatic patch effect has been subtracted.

In this context, it is important to discuss carefully all possible sources of systematic effects, in particular the effect of electrostatic patches already discussed for various high precision measurements [10–23], and more recently in the context of Casimir force measurements [24–30]. The patch effect is due to the fact that the surface of a metallic plate is made of microcrystallites with different work functions [31]. For clean metallic surfaces studied by the techniques of surface physics, the resulting voltage roughness is correlated to the grain size as well as to the orientation of microcrystallites [32]. For surfaces exposed to air, the situation is changed due to the unavoidable contamination by adsorbents, which spread out the electrostatic patches, enlarge correlation lengths, and reduce voltage dispersions [33–35].

The force due to electrostatic patches can be computed by solving the Poisson equation, as soon as the correlations of the patch voltages are known. In other words, the force depends on the associated voltage correlation function $C(\mathbf{k})$, with $\mathbf{k}$ a patch wave vector. In many studies devoted to this question, the spectrum was assumed to be flat between two sharp cutoffs at minimum and maximum wave vectors [24]. Assuming that these cutoffs are given by the grain size distribution measured with an atomic force microscope (AFM), it was concluded that the patch pressure was much smaller than the difference between the experimental Casimir pressure [more precise discussion below; see Eq. (1)] and the theoretical prediction based on the Drude model [1].

A quasilocal model was proposed recently as a better motivated representation of patches [29]. The model produces a smooth spectrum which leads to conclusions differing from those drawn from the sharp-cutoff model, due to the contribution of low values of $|\mathbf{k}|$. Using a very simple model with a uniform distribution $\mathcal{P}(\ell)$ of patch sizes ℓ up to a largest value $\ell^{\rm max}$ and a root-mean-square (rms) voltage dispersion $V_{\rm rms}$, it was found that the difference $\Delta P(D)$ between experiment and theory based on the Drude model could be qualitatively reproduced by fitting the model to the experimental data. The corresponding values for $\ell^{\rm max}$ and $V_{\rm rms}$ are different from those obtained by identifying patch and grain sizes, with $\ell^{\rm max} \sim 1$ μm larger than the maximum grain size ∼300 nm, and $V_{\rm rms} \sim 12$ mV smaller than the

*Present address: Halliburton Energy Services, Houston, Texas 77032, USA.

 ©2014 American Physical Society

rms voltage ∼80 mV associated with random orientations of clean microcrystallites of gold [1]. These values are however compatible with a contamination of metallic surfaces, which has to be expected anyway [33–35].

The results of [29] imply that patches have to be considered as an important source of systematic effects in Casimir force measurements. However, they do not prove that patches are the explanation of the difference $\Delta P(D)$ observed in [1–4]. In order to address this possibility, one has to measure the surface voltage distribution on the samples used in Casimir experiments. The method is to use the dedicated technique of Kelvin probe force microscopy (KPFM) which has the ability of achieving the necessary size and voltage resolutions [36–39]. Using the measurements of patch potential distribution, it is then possible to evaluate the contribution of the patches to the Casimir measurements and to subtract it when comparing theory and experiments. This evaluation has to be done in the plane-sphere geometry by using results in [30].

The purpose of this paper is to present the first results of such an analysis with measurements performed on the same Au-coated planar sample used to measure the Casimir interaction in a sphere-plane geometry. The paper is organized as follows. In Sec. II we briefly review Casimir measurements on gold samples performed at Indiana University–Purdue University Indianapolis (IUPUI). Section III presents normal pressure KPFM measurements of the same gold samples. These measurements are carried out independently and cross-checked in two separate laboratories, the one at IUPUI and another one at Istituto per la Sintesi Organica e la Fotoreattivitá (ISOF) in Bologna. We discuss the sample preparation and characterization, as well as the measurement of the patch properties. In Sec. IV we use the measured patch distribution to compute the electrostatic interaction in the sphere-plane geometry of Casimir experiments. As this is experimentally more difficult, we have not performed KPFM measurements on the spherical plates. We have instead used properties demonstrated in [30] to evaluate the patch force by considering that the patch properties on the curved surface are similar to those on the planar one. Within the aforementioned caveats, the main conclusion of our study, discussed in Sec. V, is that the calculated patch interaction does not have the magnitude nor distance dependence which would explain the difference $\Delta P(D)$ for the measurements reported in [1–3].

II. CASIMIR EFFECT MEASUREMENTS

A planar sample was made by sputtering 130 nm Au on a Si substrate. Morphology and roughness studies performed by atomic force microscopy indicate excellent uniformity and low roughness on the sample. The planar sample used in this paper is one of the many made for the experiments reported in [40]. The measured Casimir interaction observed in this sample is indistinguishable within the experimental error from the results reported in [2,3]. The experimental setup for measuring the Casimir effect is similar to the one used in previous work [1–3]. A Au-coated sapphire sphere [radius $R = (151.7 \pm 0.2)$ μm], is attached to a micromechanical torsional oscillator. To enhance adhesion between the ∼200 nm thick Au and the sapphire, a thin (∼10 nm) layer of Cr is first deposited on the sphere. The Au layers in both the sphere and the sample are thick enough to be considered infinite from the Casimir interaction's standpoint.

The sample is mounted on a flat platform which has an optical fiber rigidly attached to it. The fiber axis coincides with the normal of the sample-platform structure. The fiber is part of a two-color interferometer which keeps the sphere-sample separation D stable within half a nanometer. As the sample is brought into close proximity of the sphere, the interaction between the two surfaces produces a shift in the resonance frequency of the oscillator, which is used to extract the gradient of the Casimir force, $\partial_D F_C$. The use of a sphere instead of another planar surface avoids the problem of keeping the two objects parallel but complicates the exact theoretical description. A common approach to bypass this difficulty relies on the proximity force approximation. When $D/R \ll 1$, one can then approximate the sphere's surface as a collection of planar elements. Within this procedure, the force gradient can be calculated as the sum of several local parallel plane interactions, and

$$\partial_D F_C(D) = 2\pi R P_{pp}(D), \tag{1}$$

where $P_{pp}(D)$ is the Lifshitz expression for the Casimir pressure between two parallel plates [41].

As customarily done in Casimir force measurements [1–3,42,43], the apparatus was calibrated using a calculable interaction, i.e., the electrostatic interaction between the sphere and the sample. In this section, we assume the two objects to be equipotentials, so that the electrostatic energy between them is given by

$$E_e(D) = \tfrac{1}{2} C(D) \Delta V^2, \tag{2}$$

where $C(D)$ is the capacitance between the sphere and the plane separated by a distance D, and the potential difference between them $\Delta V = V_s - V_p$. An external voltage V_0 is applied between the two surfaces in the calibration process [1–3,42,43], so that the potential difference becomes $\Delta V - V_0$.

From Eq. (2) the force and the gradient of the force can be easily derived when ΔV is not a function of distance. In the calibration process both the expression of the force and the gradient of the force have been used. It turns out [1–3] that the force

$$F_e(D) = \frac{1}{2} \frac{\partial C(D)}{\partial D} (\Delta V - V_0)^2, \tag{3}$$

and the gradient of the force

$$\partial_D F_e(D) = \frac{1}{2} \frac{\partial^2 C(D)}{\partial D^2} (\Delta V - V_0)^2, \tag{4}$$

are not zero when $\Delta V = 0$. With the simple Eqs. (3) and (4) corresponding to equipotential surfaces, the electrostatic interaction can be made null by a judicious choice of the applied potential chosen to cancel the initial potential $V_0 = V_{\min} = \Delta V$ ($V_{\min}$ is called the "minimizing potential"). A more precise discussion taking into account the patch effect will be given below, in Sec. IV.

In our calibration procedure, we have found that by taking the derivative with respect to the potential difference, $V_{\min}$ is more accurately determined [44]. Either the use of the

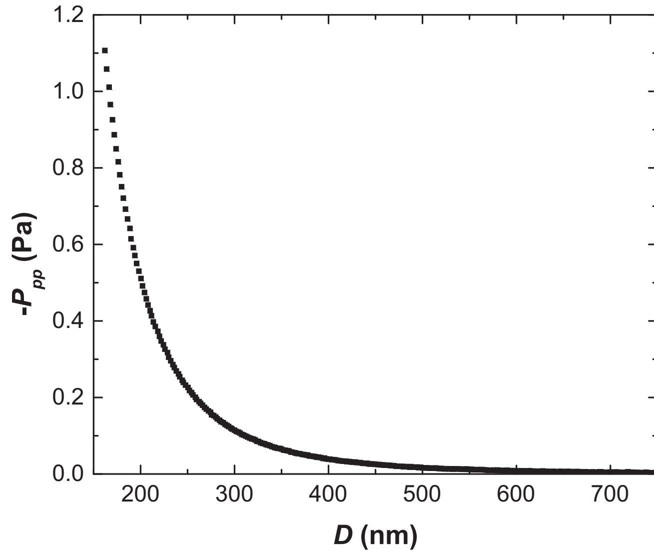

FIG. 1. Equivalent Casimir pressure as a function of separation between the sphere and the sample. Error bars in P ($\lesssim$3 mPa) and D ($\sim$0.5 nm) are too small to be seen.

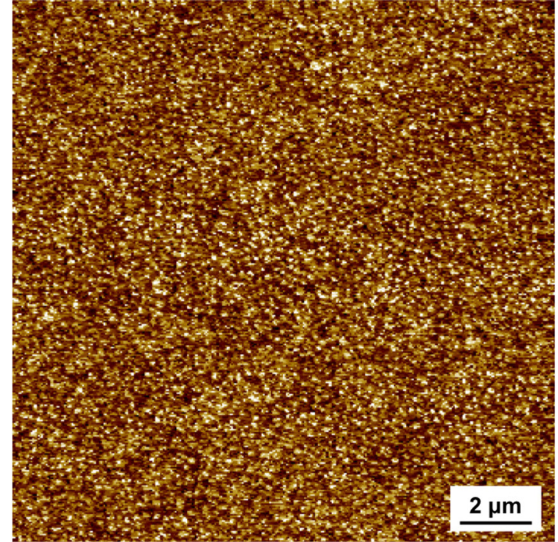

FIG. 2. (Color online) KPFM image of the electrostatic potential distribution $V_p(\mathbf{x})$ on the surface of the Au sample recorded at ISOF. This image is composed of 512×512 pixels, with a lateral size of 15.36 μm. The scale bar corresponds to 2 μm and the scan range is 20 mV. The amplitude of the modulation is $V_1 = 2.5$ V.

electrostatic force or the gradient of the electrostatic force yield the same calibration parameters and, relevant for this paper, the same value of $V_{\min}$. This minimizing potential was found to be independent of D within the experimental accuracy of 0.1 mV. The results of the Casimir interaction between the sphere and the sample are shown in Fig. 1.

III. KPFM MEASUREMENTS

The electrostatic potential distribution $V_p(\mathbf{x})$ on the Au sample surface is measured by Kelvin probe force microscopy. This contactless technique is based on monitoring long-ranged electrostatic interactions between a cantilever and a sample. A sharp metal-coated tip is microfabricated at the edge of a cantilever which is maintained at a fixed potential. With no mechanical action of the tip on the sample, electrostatic forces exerted on the cantilever are measured, just as in AFM, by the deflection of the cantilever using the reflection of a laser beam off the tip [39,45]. Because these forces are proportional to the variation with distance D of the local capacitance C between the tip and the sample, a direct quantification of the surface potential difference ΔV between the tip and the sample is not trivial. To achieve this, KPFM measurements exploit a Zeeman vibrating capacitor setup [36]. The two electrodes of the capacitor are the sample and the tip which is forced to oscillate at a fixed frequency ω while raster-scanning the surface of the sample at fixed separation distance D. In such an amplitude modulation (AM) mode, which is used for all KPFM measurements reported in this paper, the tip oscillations modulate the tip-sample electrostatic interaction energy $U(D) = \frac{1}{2}C\Delta V^2$, assuming a linear relationship between local charges and local potentials [46]. The electrical potential inhomogeneities of the surface sample can thus be mapped by detecting the amplitude variations of the free tip oscillations.

More precisely, a feedback loop applies an adjustable DC bias offset potential V_0 to the cantilever tip in order to minimize the interaction between the tip and the sample. Superimposed to this DC voltage bias, an alternating current (AC) signal is applied to the tip harmonically at a frequency ω. In this case, ΔV is replaced in the expression for the interaction energy by the total voltage $\Delta V - V_0 + V_1 \sin(\omega t)$ between the tip and the sample, where V_1 is the amplitude of the modulation. Then, the ω component of the resulting force $F_\omega = -\partial_D U_\omega = -\partial_D C\,[(\Delta V - V_0)\, V_1 \sin(\omega t)]$, directly measured with a lock-in amplifier, is canceled when $V_0 = \Delta V$. The feedback circuit monitors the bias V_0 applied to compensate for the surface potential ΔV, thus providing a direct quantification of the latter. Note that the tip potential is calibrated using HOPG (high ordered pyrolytic graphite), a substrate very stable in air. This calibration implies that the real potential $V_p(\mathbf{x})$ on the sample is determined up to a constant value (at a fixed tip-sample distance). Such an offset does not affect the measurement of the variations of the surface potential (see Sec. IV below for a more precise discussion).

The KPFM measurements shown in Fig. 2 have been performed at ISOF using a commercial microscope Multimode III (Bruker) equipped with an Extender Electronics module. The measurements have been acquired in a nitrogen environment (relative humidity smaller than 10%) at room temperature. Potential maps have been recorded over a surface area of 15.36×15.36 μm^2, with 512 pixels per line, using a scanning rate of 1 Hz per line. In order to obtain a sufficiently large and detectable mechanical deflection of the microscope tip, we used a 20 nm radius Pt/Ir coated Si ultra levers (SCM, Bruker) with oscillating frequencies $\omega \sim (75 \pm 15)$ kHz and stiffness $k \sim 2.8$ N m^{-1}. The measurements have been performed at a fixed tip-sample distance $D = 30$ nm, chosen as the minimal

distance that prevents artifacts due to the cross-talking between topographic and electrical signals (precise criterion below).

Similar results were obtained at IUPUI using a different AFM (Brueker Dimension) with 20 nm radius Cr/Pt coated Si levers (Budget Sensors, TAP190E-G) under similar environmental conditions. These cantilevers are stiffer, with $k \sim 48$ N m^{-1} and a resonance frequency $\sim(190 \pm 30)$ kHz. The KPFM measurements were performed over a smaller area of 5×5 μm^2, with 256 points per line and at 1 Hz per line. The measurements were repeated at different separations and it was found that the results from 20 to 60 nm were compatible and reproducible when V_1 was kept below 3 V, without any cross-talk artifacts.

The criterion for the avoidance of cross-talking in both cases (IUPUI and ISOF) is the observation of not too large correlations $\langle h(x,y)\Delta V(x,y)\rangle < 0.5$ between the height $h(x,y)$ measured by the AFM at point (x,y) and the potential $\Delta V(x,y)$ measured by the KPFM at the same point.

Obviously, the measured KPFM image is a convolution between the real potential map and the microscope transfer function, leading to unavoidable broadening of the nano-objects and underestimation of the measured potential differences. The measured map can be retrieved using linear deconvolution, although perfect recovery is impossible without a precise description of the noise in the system [47,48]. The transfer function can be described in terms of tip-sample electrostatic interactions and its width corresponds to effective surface area of the sample interacting with the tip. Due to the long-range nature of the electrostatic interactions, the area of the surface sampled in such a measurement expands several tens of nanometers beyond the area underneath the apex of the probe. In addition, the surrounding part of the conical tip as well as the oscillating cantilever contribute to the interaction. Other experimental parameters, in particular the amplitude V_1 of the modulation, affect the transfer function and its analytic evaluation requires a comprehensive simulation of the tip-sample system [49]. Usually, the transfer function has been calculated using simplified tip geometries [50,51].

In this work, we have bypassed simulations and simplified geometries by exploiting a semiquantitative model developed in Ref. [39]. This approach has been checked by measuring nano-patterned samples with well-defined geometries. Previous experiments performed with the same tip-sample geometry at the same separation distance allowed us to evaluate an effective microscope transfer function width of $\sim$100 nm [37]. In the case of an isotropic surface, the transfer function can be assumed to be Gaussian. In this situation, a simple relation $w = 0.626 \times L_R$ was recently demonstrated between the width (w) of the effective area and lateral resolution (L_R) defined as the minimal detectable feature size [38,52]. For ISOF measurements, the pixel size of 30 nm corresponds to a third of the effective area width. This allows us to neglect pixelization and convolution artifacts for areas larger than 160 nm (i.e., larger than 5 pixels width), and implies that the acquired KPFM images provide us with fair maps of the gold surface potential for patch sizes larger than 160 nm. We tested this property by using the same KPFM experimental setup to measure the electrical potential of interdigitated gold nanoelectrodes having a channel length and an electrode width of 200 nm. By comparing the applied potential and the measured one, we observed an underestimation of the electrical potential difference with AM-KPFM of the order of 20%.

IV. ELECTROSTATIC PATCH INTERACTION BETWEEN A PLANE AND A SPHERE

In the following we recall the basic equations to evaluate the electrostatic patch interaction between a plane and a sphere, using the exact solutions derived in [30]. In particular, the known case of perfect equipotential surfaces on the plane and the sphere can be solved in this way (see Appendix C in [30]). Here we write the exact solutions for patchy surfaces, and show how to deduce the patch interaction from the KPFM data measured on the gold samples. Writing this interaction as an equivalent pressure, as in Eq. (1), we finally compare our results to $\Delta P(D)$.

In order to solve the Poisson equation in the sphere-plane geometry with arbitrary potential distributions on both surfaces, it is advantageous to use bispherical coordinates because the equation is then separable and the surfaces correspond to constant values of the bispherical coordinate η [30]. Writing the boundary value problem for the electrostatic potential in the space between the sphere and the plane, the interaction energy can be expressed as a double integration over solid angles in bispherical coordinates, $\int d\Omega \equiv \int_0^\pi d\xi \int_0^{2\pi} d\phi \sin\xi$, of a quadratic form of the surface potentials (see Eq. (11) of [30]). After performing a coordinate transformation from bispherical to spherical or polar coordinates, appropriate for the spherical and planar surfaces respectively, the integration energy can be written in the form

$$E_{\rm sp} = \sum_{a,b} \iint d\Omega_a d\Omega_b V_a(\Omega_a)\mathcal{E}_{a,b}(\Omega_a;\Omega_b)V_b(\Omega_b), \quad (5)$$

where $V_{a,b}(\Omega_{a,b})$ denote the arbitrary electrostatic potentials on the sphere and the plane (with $a,b =$ s or p respectively), $\Omega_{\rm s} \equiv (\theta,\phi)$ are spherical coordinates on the sphere, and $\Omega_{\rm p} \equiv (\rho,\phi)$ are polar coordinates on the plane. The integration measures are defined as $\int d\Omega_{\rm s} = \int_0^{2\pi} d\phi \int_0^\pi d\theta \sin\theta$ (here θ is a polar angle on the sphere) and $\int d\Omega_{\rm p} = \int_0^{2\pi} d\phi \int_0^\infty d\rho\, \rho$ (here ρ is the radius for a polar coordinate system defined on the plane with origin below the apex of the sphere). The kernels $\mathcal{E}_{a,b}(\Omega_a;\Omega_b)$ depend on the distance D between the sphere and the plane, and their explicit expressions are given in Appendix B of [30]. By taking the derivative of the energy (5) with respect to D, the electrostatic patch force between the sphere and the plane is computed:

$$F_{\rm sp} = \sum_{a,b} \iint d\Omega_a d\Omega_b V_a(\Omega_a)\mathcal{F}_{a,b}(\Omega_a;\Omega_b)V_b(\Omega_b),$$
$$\mathcal{F}_{a,b}(\Omega_a;\Omega_b) = \frac{\partial \mathcal{E}_{a,b}(\Omega_a;\Omega_b)}{\partial D}. \quad (6)$$

This expression is general for arbitrary boundary conditions on the sphere and the plane.

As explained in Sec. III, we have measured the patch voltages on the planar Au samples used in our Casimir force measurements, but we do not have the same KPFM experimental knowledge for the sphere used in Casimir experiments. In this context, we use the following strategy to compute the

total patch force. We consider that the patch properties on the weakly curved surface ($R \gg D$) are similar to those on the planar one on the length scales of relevance for our calculation, and we use the fact known from [30] that the kernels $\mathcal{E}_{s,s}$ and $\mathcal{E}_{p,p}$ thus lead to similar contributions (again for $R \gg D$). We also assume that there are no statistical correlations between the patches on the sphere and the plane ($\langle V_s(\Omega_s)V_p(\Omega_p)\rangle = 0$), so that the kernel $\mathcal{E}_{s,p}$ leads to a negligible contribution. We then approximate the total force between the plane and the sphere as twice the patch interaction calculated in the simpler case when the sphere is grounded ($V_s = 0$) and the plane has the patch distribution known from measurements

$$F_{sp} \approx 2 \iint d\Omega_p d\Omega'_p V_p(\Omega_p)\mathcal{F}_{p,p}(\Omega_p;\Omega'_p)V_p(\Omega'_p). \quad (7)$$

We expect that this approximate expression for the patch force gives the correct order of magnitude and distance dependence for the patch interaction, provided the patch properties on the sphere and the plane are similar, and the cross-terms between the sphere and the plane have a negligible contribution.

As discussed in Sec. II, an external voltage V_0 is applied between the two surfaces in order to perform the electrostatic calibration of the system. This bias V_0 is swept to observe the quadratic dependence of (3) or (4) on V_0 at fixed sphere-plane separation D, and obtain its minimum which defines the minimizing potential

$$0 = \left.\frac{\partial F_{sp}}{\partial V_0}\right|_{V_0=V_{min}}. \quad (8)$$

A precise description of this problem is built up by adding a constant value V_0 to the patchy potential V_p in (7) and sweeping it. Solving (8), we find that V_{min} is defined so that it compensates exactly the average value $\overline{V}_p$ of the patch potential over the zone of electrostatic influence, with the latter defined from the kernel $\mathcal{F}_{p,p}$ [30]:

$$V_{min} = -\overline{V}_p, \quad \overline{V}_p \equiv \frac{\int d\Omega_p \int d\Omega'_p V_p(\Omega_p)\mathcal{F}_{p,p}(\Omega_p;\Omega'_p)}{\int d\Omega_p \int d\Omega'_p \mathcal{F}_{p,p}(\Omega_p;\Omega'_p)}. \quad (9)$$

The size of the zone of electrostatic influence is of the order of $\sqrt{RD} \sim 10\ \mu$m, with the numbers corresponding to the experiments in [1–3]. The minimizing potential V_{min}, which depends of the specific realization of the patch voltage in the zone of electrostatic influence, has to vary when the sphere-plane separation or the lateral position of the sphere above the plane are changed. However, this variation can be small due to the averaging of the effect of patches over the zone of electrostatic influence.

With the more complete treatment of the electrostatic problem now achieved, setting the applied potential V_0 equal to V_{min} does no longer nullify the electrostatic interaction between the sphere and the plane, but only minimizes it. There indeed remains the effect of the dispersion of the patchy potential V_p over the zone of electrostatic influence. This statement is made quantitative by evaluating the residual patch force (7) which remains at the minimizing potential (9):

$$\begin{aligned} F_{res} &\equiv F_{sp}|_{V_0=V_{min}} \\ &= 2 \iint d\Omega_p d\Omega'_p \delta V_p(\Omega_p)\mathcal{F}_{p,p}(\Omega_p;\Omega'_p)\delta V_p(\Omega'_p). \end{aligned} \quad (10)$$

Here $\delta V_p(\Omega_p)$ is the deviation of the patchy potential from its average over the zone of electrostatic influence,

$$\delta V_p(\Omega_p) \equiv V_p(\Omega_p) - \overline{V_p}, \quad (11)$$

so that the residual patch force can effectively be regarded as measuring the dispersion of $\delta V_p(\Omega_p)$ over the zone of electrostatic influence.

At this point, it is worth discussing the contribution of patches corresponding to given size scales. For small sizes, smaller than the distance D between the two plates, the contribution is suppressed by the kernel $\mathcal{F}_{p,p}$ obtained by solving the Poisson equation. For large sizes, larger than the size $\sqrt{RD}$ of the zone of electrostatic influence, the contribution could be large before the calibration process, but it is essentially canceled out in this process because V_{min} is defined so that it compensates the average potential of patches over this zone. It follows that the significant contributions are mainly associated to size scales in the intermediate interval from D to $\sqrt{RD}$, that is from a fraction of a μm to 10 μm with the numbers corresponding to the experiments in [1–3]. These qualitative statements are made precise by using the Eq. (10), with the expression of the kernel $\mathcal{F}_{p,p}$ taken from [30].

When performing numerical evaluations, we have to face the difficulty that the measured samples are, of course, finite, as discussed in Sec. III. In order to obtain patch distribution data over a sufficiently large area, we used the following "mirror symmetry + replica" procedure. We took the measured KPFM data of the finite-size square sample (we call it 1×1 cell), generated a 2×2 cell by taking mirror images of the original 1×1 cell, and then the 2×2 cell was periodically replicated on two dimensions, until the final size reached $80 \times 80\ \mu\text{m}^2$, which is certainly enough for our numerics. Clearly, this procedure introduces artificial correlations over distances larger than the original sample sizes ($15 \times 15\ \mu\text{m}^2$ for the larger ones), and it also ignores possible long-distance correlations associated with very large patches. We believe our method to be valid, at least for preliminary estimations, as a consequence of the discussion of the preceding paragraph. The contribution of possibly large patches (with sizes larger than $\sqrt{RD}$) is essentially washed out in the electrostatic calibration process because V_{min} compensates the average potential of patches over the zone of electrostatic influence. We computed the voltage correlation function from the KPFM data, and the resulting correlation within the measurement area decreases as a function of distance in an approximate exponential form. This supports our assumption above for computing the electrostatic patch interaction.

Figure 3 shows our numerical results for the patch interaction, measured as an equivalent patch pressure as in Eq. (1). Though they were obtained on different parts of the same sample with different instruments, scan sizes and resolutions, the measurements made at IUPUI (solid line with squares) and ISOF (dashed line with circles) lead to comparable patch pressures, in terms of their magnitude and variation with distance. In particular, both curves have a different law of variation with D and smaller magnitudes than $\Delta P(D)$, also reproduced for comparison on Fig. 3. For this difference, the bars show the experimental uncertainties discussed in [2,3],

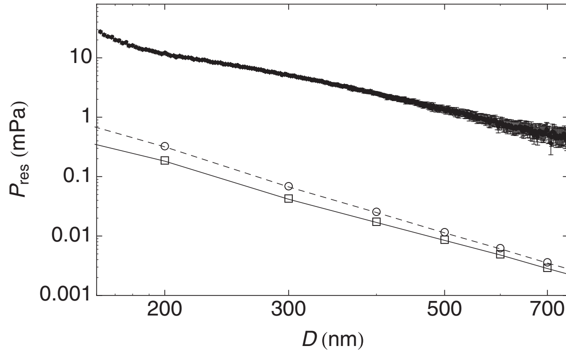

FIG. 3. Equivalent electrostatic patch pressure P_{res} computed for the IUPUI (solid line with squares) and ISOF (dashed line with circles) data, versus distance D. We also show, for comparison, the difference $\Delta P(D)$ between experimental measurements of the Casimir pressure and theoretical predictions based on the Drude model.

similar to those shown in Fig. 1. The theoretical calculations from the Drude model are described in [1,2,29]. They are done at room temperature $T = 295$ K using tabulated optical data extrapolated to low frequencies with a Drude model with parameters $\Omega_P = 8.9$ eV for the plasma frequency and $\gamma = 0.0357$ eV for the damping rate. A simple model for roughness corrections is used [2], with root-mean-square roughness heights of 3.6 and 1.9 nm, for the plane and the sphere respectively.

V. CONCLUSIONS

In this paper, we have shown that it is possible to measure patch properties on the same Au samples used in Casimir experiments [2,3]. In fact we did it on the planar samples and we assumed that the properties were similar on the spherical ones. We then estimated the contribution of patches to the force in the plane-sphere geometry used in Casimir experiments [30].

We have discussed the subtleties associated to small and large patch sizes. The influence of patch sizes smaller than the plane-sphere distance D is suppressed in the solution of the Poisson equation. The influence of patch areas larger than the zone of influence $2\pi RD$ is canceled by the voltage V_0 applied in the electrostatic calibration. This entails that, for the parameters used in the Casimir experiment, the significant contributions from patches are mainly associated with sizes in the interval from a fraction of a μm to $\sim$10 μm. Hence the resolution of the AM-KPFM measurements discussed in Sec. III should be sufficient for a reliable estimation of the effect of electrostatic patches shown in Sec. IV.

The patch pressure estimations shown in Fig. 3 have smaller magnitudes and a different law of variation with D than the difference $\Delta P(D)$ observed in Casimir experiments [2,3]. They do not reproduce the results which were found in [29] to fit this difference. This means that the statistical properties measured on the patches differ from the model used in [29]. We also emphasize at this point that the description of the patch interaction in [29] was based on the proximity force approximation, whereas the present paper used the much more satisfactory approach developed in [30] to perform precise evaluations in the plane-sphere geometry.

The analysis of the present paper is preliminary and some of its limitations have to be cured by further work. In our calculation of the sphere-plane patch force (7), we have assumed that the patches on the sphere had the same statistical properties as on the plane, and also that the cross-correlations between the patches on the sphere and plane had a negligible contribution. In order to confirm these assumptions, it would be necessary to measure patches on the spherical mirrors, which is an experimental challenge. We have measured patch distributions on samples at ambient pressures, whereas the Casimir experiments were performed at $\sim 10^{-7}$ torr. As the pressure could influence the contamination process and hence the patch properties, it would be crucial to repeat the patch characterization on the same metallic samples and under the same environmental conditions as in the vessel where Casimir measurements are done.

Our KPFM measurements were done with a scan size of the order of 15 μm and a resolution of the order of 160 nm (ISOF experiment). Such numbers should be sufficient to get a qualitative characterization, as they cover the patch sizes having a critical influence on the force between the plane and the sphere. Of course, larger scan sizes and improved resolutions would allow one to test the reliability and accuracy of the whole method. Further work is thus needed to confirm the present result that the patch contribution does not match the difference $\Delta P(D)$ observed in Casimir experiments [1–4].

Note added. While this paper was under review, a preprint [53] has become available with conclusions differing from ours. It is asserted there that AM-KPFM measurements underestimate the potential differences as measured by frequency modulation (FM) KPFM and thus lead only to a lower bound for the patch contribution to the force. Underestimations by AM-KPFM of the true potential differences on metallic samples have indeed been reported [54], and they depend on experimental conditions. As explained at the end of Sec. III, we have checked that the underestimation is of the order of 20% for typical patch sizes of 200 nm and under the experimental conditions used in our measurements. Though it calls for further work in order to confirm the results of the present paper, such an underestimation does not affect its conclusions (see the preceding paragraphs).

ACKNOWLEDGMENTS

The authors thank the participants to the ESF Research Networking Programme CASIMIR (http://www.casimir-network.org) for many discussions related to the topic of this paper. Work at Los Alamos National Laboratory was carried out under the auspicies of the LDRD program. This work was performed, in part, at the Center for Nanoscale Materials, a U.S. Department of Energy, Office of Science, Office of Basic Energy Sciences User Facility under Contract No. DE-AC02-06CH11357. R.S.D. acknowledges support from the IUPUI Nanoscale Imaging Center, Integrated Nanosystems Development Institute, Indiana University Collaborative Research Grants, and the Indiana University Center for Space Symmetries.

[1] R. S. Decca, D. López, E. Fischbach, G. L. Klimchitskaya, D. E. Krause, and V. M. Mostepanenko, Ann. Phys. (NY) **318**, 37 (2005).
[2] R. S. Decca, D. López, E. Fischbach, G. L. Klimchitskaya, D. E. Krause, and V. M. Mostepanenko, Phys. Rev. D **75**, 077101 (2007).
[3] R. S. Decca, D. López, E. Fischbach, G. L. Klimchitskaya, D. E. Krause, and V. M. Mostepanenko, Eur. Phys. J. C **51**, 963 (2007).
[4] C.-C. Chang, A. A. Banishev, R. Castillo-Garza, G. L. Klimchitskaya, V. M. Mostepanenko, and U. Mohideen, Phys. Rev. B **85**, 165443 (2012).
[5] K. A. Milton, J. Phys. A **37**, R209 (2004).
[6] G. L. Klimchitskaya, U. Mohideen, and V. M. Mostepanenko, Rev. Mod. Phys. **81**, 1827 (2009).
[7] G.-L. Ingold, A. Lambrecht, and S. Reynaud, Phys. Rev. E **80**, 041113 (2009).
[8] I. Brevik and J. S. Høye, Eur. J. Phys. **35**, 015012 (2014).
[9] A. O. Sushkov, W. J. Kim, D. A. R. Dalvit, and S. K. Lamoreaux, Nat. Phys. **7**, 230 (2011).
[10] F. C. Witteborn and W. M. Fairbank, Phys. Rev. Lett. **19**, 1049 (1967).
[11] J. B. Camp, T. W. Darling, and R. E. Brown, J. Appl. Phys. **69**, 7126 (1991).
[12] V. Sandoghdar, C. I. Sukenik, S. Haroche, and E. A. Hinds, Phys. Rev. A **53**, 1919 (1996).
[13] Q. A. Turchette, D. Kielpinski, B. E. King, D. Leibfried, D. M. Meekhof, C. J. Myatt, M. A. Rowe, C. A. Sackett, C. S. Wood, W. M. Itano, C. Monroe, and D. J. Wineland, Phys. Rev. A **61**, 063418 (2000).
[14] L. Deslauriers, S. Olmschenk, D. Stick, W. K. Hensinger, J. Sterk, and C. Monroe, Phys. Rev. Lett. **97**, 103007 (2006).
[15] N. A. Robertson, J. R. Blackwood, S. Buchman, R. L. Byer, J. Camp, D. Gill, J. Hanson, S. Williams, and P. Zhou, Class. Quantum Grav. **23**, 2665 (2006).
[16] R. J. Epstein, S. Seidelin, D. Leibfried, J. H. Wesenberg, J. J. Bollinger, J. M. Amini, R. B. Blakestad, J. Britton, J. P. Home, W. M. Itano, J. D. Jost, E. Knill, C. Langer, R. Ozeri, N. Shiga, and D. J. Wineland, Phys. Rev. A **76**, 033411 (2007).
[17] S. E. Pollack, S. Schlamminger, and J. H. Gundlach, Phys. Rev. Lett. **101**, 071101 (2008).
[18] R. Dubessy, T. Coudreau, and L. Guidoni, Phys. Rev. A **80**, 031402 (2009).
[19] J. D. Carter and J. D. D. Martin, Phys. Rev. A **83**, 032902 (2011).
[20] C. W. F. Everitt, D. B. DeBra, B. W. Parkinson, J. P. Turneaure, J. W. Conklin, M. I. Heifetz, G. M. Keiser, A. S. Silbergleit, T. Holmes, J. Kolodziejczak, M. Al-Meshari, J. C. Mester, B. Muhlfelder, V. G. Solomonik, K. Stahl, P. W. Worden, Jr., W. Bencze, S. Buchman, B. Clarke, A. Al-Jadaan, H. Al-Jibreen, J. Li, J. A. Lipa, J. M. Lockhart, B. Al-Suwaidan, M. Taber, and S. Wang, Phys. Rev. Lett. **106**, 221101 (2011).
[21] R. D. Reasenberg, E. C. Lorenzini, B. R. Patla, J. D. Phillips, E. Popescu, E. Rocco, and R. Thapa, Class. Quantum Grav. **28**, 094014 (2011).
[22] D. A. Hite, Y. Colombe, A. C. Wilson, K. R. Brown, U. Warring, R. Jordens, J. D. Jost, K. S. McKay, D. P. Pappas, D. Leibfried, and D. J. Wineland, Phys. Rev. Lett. **109**, 103001 (2012).
[23] D. A. Hite, Y. Colombe, A. C. Wilson, D. T. C. Allcock, D. Leibfried, D. J. Wineland, and D. P. Pappas, MRS Bulletin **38**, 826 (2013).
[24] C. C. Speake and C. Trenkel, Phys. Rev. Lett. **90**, 160403 (2003).
[25] A. A. Chumak, P. W. Milonni, and G. P. Berman, Phys. Rev. B **70**, 085407 (2004).
[26] W. J. Kim, A. O. Sushkov, D. A. R. Dalvit, and S. K. Lamoreaux, Phys. Rev. A **81**, 022505 (2010).
[27] W. J. Kim and U. D. Schwarz, J. Vac. Sci. Technol. B **28**, C4A1 (2010).
[28] S. de Man, K. Heeck, R. J. Wijngaarden, and D. Iannuzzi, J. Vac. Sci. Technol. B **28**, C4A25 (2010).
[29] R. O. Behunin, F. Intravaia, D. A. R. Dalvit, P. A. Maia Neto, and S. Reynaud, Phys. Rev. A **85**, 012504 (2012).
[30] R. O. Behunin, Y. Zeng, D. A. R. Dalvit, and S. Reynaud, Phys. Rev. A **86**, 052509 (2012).
[31] R. Smoluchowski, Phys. Rev. **60**, 661 (1941).
[32] N. Gaillard, M. Gros-Jean, D. Mariolle, F. Bertin, and A. Bsiesy, Appl. Phys. Lett. **89**, 154101 (2006).
[33] F. Rossi and G. I. Opat, J. Appl. Phys. D **25**, 1349 (1992).
[34] T. W. Darling, F. Rossi, G. I. Opat, and G. F. Moorhead, Rev. Mod. Phys. **64**, 237 (1992).
[35] T. C. Leung, C. L. Kao, W. S. Su, Y. J. Feng, and C. T. Chan, Phys. Rev. B **68**, 195408 (2003).
[36] M. Nonnenmacher, M. P. Oboyle, and H. K. Wickramasinghe, Appl. Phys. Lett. **58**, 2921 (1991).
[37] A. Liscio, V. Palermo, K. Müllen, and P. Samori, J. Phys. Chem. C **112**, 17368 (2008).
[38] A. Liscio, V. Palermo, and P. Samori, Adv. Func. Mater. **18**, 907 (2008).
[39] A. Liscio, V. Palermo, and P. Samori, Accounts Chem. Res. **43**, 541 (2010).
[40] F. Intravaia, S. Koev, I. W. Jung, A. A. Talin, P. S. Davids, R. S. Decca, V. A. Aksyuk, D. A. R. Dalvit, and D. López, Nat. Commun. **4**, 2015 (2013).
[41] E. M. Lifshitz, Sov. Phys. JETP **2**, 73 (1956).
[42] S. de Man, K. Heeck, and D. Iannuzzi, Phys. Rev. A **79**, 024102 (2009).
[43] R. S. Decca, E. Fischbach, G. L. Klimchitskaya, D. E. Krause, D. López, U. Mohideen, and V. M. Mostepanenko, Int. J. Mod. Phys. A **26**, 3930 (2011).
[44] R. S. Decca and D. López, Int. J. Mod. Phys. A **24**, 1748 (2009).
[45] W. Melitz, J. Shen, A. C. Kummel, and S. Lee, Surf. Sci. Rep. **66**, 1 (2011).
[46] H. O. Jacobs, P. Leuchtmann, O. J. Homan, and S. Stemmer, J. App. Phys. **84**, 1168 (1998).
[47] T. Machleidt, E. Sparrer, D. Kapusi, and K.-H. Franke, Meas. Sci. Technol. **20**, 084017 (2009).
[48] G. Cohen, E. Halpern, S. U. Nanayakkara, J. M. Luther, C. Held, R. Bennewitz, A. Boag, and Y. Rosenwaks, Nanotechnology **24**, 295702 (2013).
[49] D. S. H. Charrier, M. Kemerink, B. E. Smalbrugge, T. de Vries, and R. A. J. Janssen, ACS Nano **2**, 662 (2008).
[50] J. Colchero, A. Gil, and A. M. Baró, Phys. Rev. B **64**, 245403 (2001).
[51] E. Strassburg, A. Boag, and Y. Rosenwaks, Rev. Sci. Instrum. **76**, 083705 (2005).
[52] S. V. Kalinin, S. Jesse, B. J. Rodriguez, J. Shin, A. P. Baddorf, H. N. Lee, A. Borisevich, and S. J. Pennycook, Nanotechnology **17**, 3400 (2006).
[53] J. L. Garret, D. Somers, and J. N. Munday, arXiv:1409.5012.
[54] U. Zerweck, C. Loppacher, T. Otto, S. Grafström, and L. M. Eng, Phys. Rev. B **71**, 125424 (2005).